

## 16.1 DIAGNOSING TRANSPORT AND MIXING IN UNSTEADY FLOWS USING TRANSIT TIME DISTRIBUTION

Hong Zhang\*, Thomas W.N. Haine and Darryn W. Waugh  
Dept. of Earth and Planetary Sci., The Johns Hopkins University, Baltimore, MD

### 1. INTRODUCTION

The past decades have seen an enormous expansion in the number of observations of chemical tracers in the ocean (England and Maier-Reimer, 2001). This has resulted in a better understanding of ocean ventilation rates, water-mass formation processes and pathways of interior flow. Recently, there has been a lot of research regarding the timescales derived from tracers (tracer ages) and their relationship to transport (Holzer and Hall, 2000; Haine and Hall, 2002). A generalized transport theory has been established for water-mass composition and tracer ages. The framework of the transport theory is based on the age spectrum (Green's function) which contains tracer-independent information on transport processes.

In a diffusive geophysical flow, there is not a single timescale or unique pathway for transport from the surface into the interior because of irreversible mixing processes. Instead, there is a range of pathways and hence a distribution of transit times. Such a distribution of transit times since last surface contact is called the age spectrum, or transit time distribution. Mathematically, it is a type of Green's function that propagates a boundary condition of the tracer at a surface into the interior. Given the age spectrum, it is possible to determine the temporal variations of a tracer with known surface concentration. Analytical expressions for the age spectrum are available for simple flows, for example, one dimensional flow with constant advection and diffusion has Inverse Gaussian distribution (Hall and Plumb, 1994). For steady flow some simple relationships exist between tracer-derived ages, the ideal age, and the age spectrum (Waugh et al., 2002, Hall and Haine, 2002). In more complex flows these relationships are not known. In this study we explore this issue using a barotropic gyre circulation model as this model can provide both steady and unsteady circulation regimes. The dynamical simulations and tracer simulations are presented in the next two sections, followed by conclusion and discussion in Section 4.

### 2. DYNAMICAL SIMULATION

Mid-latitude surface ocean circulation is

---

\*Corresponding author address: Hong Zhang, The Johns Hopkins University, Dept. of Earth and Planetary Sci., 3400 N Charles St., Baltimore, MD 21218; Email: hongyan@jhu.edu

characterized by basin-wide asymmetrical gyres, which are stronger on the western side of the basin. The gyre circulation occurs over a wide range of time scales and space scales (Siedler et al., 2001). Simulations of the double gyre circulation in both shallow water models and quasi-geostrophic models show that a wide range of flows can occur (Meacham 2000, Chang et al. 2001, Ghil et al. 2002) from steady circulation to unsteady circulation as the forcing changes.

We carry out numerical experiments of a simple barotropic wind-driven double gyre circulation using the MITgcm (Marshall et al. 1997). The model is configured in a square basin on a mid-latitude  $\beta$  plane and forced by steady zonal wind stress. The governing equations are a set of shallow water equations:

$$\frac{Du}{Dt} - fv + g \frac{\partial \eta}{\partial x} - A_h \nabla^2 u = \frac{\tau_x}{\rho_0 H}$$

$$\frac{Dv}{Dt} + fu + g \frac{\partial \eta}{\partial y} - A_h \nabla^2 v = 0$$

$$\frac{D\eta}{Dt} + H \left( \frac{\partial u}{\partial x} + \frac{\partial v}{\partial y} \right) = 0$$

where the wind stress is assumed to have a simple symmetric form  $\tau_x(y) = \tau_0 \sin(\pi y/L_y)$ . The corresponding model parameters are listed in Table 1.

TABLE 1 Model parameters

Parameter	Value
Coriolis parameter	$f_0 = 10^{-4} \text{ s}^{-1}$
$f(y) = f_0 + \beta y$	$\beta = 10^{-11} \text{ m}^{-1} \text{ s}^{-1}$
Wind stress	$\tau_0 = 0.1 \text{ Pa}$
Viscosity coefficient	$A_h = 100 \text{ m}^2 \text{ s}^{-1}$
Domain extent	$L_x = L_y = 1200 \text{ km}$
Grid resolution	$\Delta x = \Delta y = 20 \text{ km}$
Time step	$\Delta t = 20 \text{ min}$

The dynamics of the wind-driven model is controlled by two nondimensional parameters (Pedlosky, 1996). They are the dimensional inertial and Munk layer thickness ( $\delta_I^*$ ,  $\delta_M^*$ ) scaled by the width of the basin:

$$\delta_I = \delta_I^* / L_x \quad \text{and} \quad \delta_M = \delta_M^* / L_x \quad \text{where}$$

$\delta_I^* = (U/\beta)^{1/2}$  and  $\delta_M^* = (A_h/\beta)^{1/3}$ . The velocity scale  $U$  in the interior and the characteristic value of wind-stress  $\tau_0$  are connected by the Sverdrup relation. For a square basin with a double gyre wind-stress the scaling leads to  $U = \pi \tau_0 / \rho_0 \beta L_y H$ . The two parameters  $\delta_I$  and  $\delta_M$  measure the importance of the nonlinearity and lateral dissipation, respectively. In

our simulation,  $\delta_i$  is changed and  $\delta_M$  fixed as in Chang et al. (2001).

To examine the dependence of the circulation on different parameters we perform 100-yr simulations where fluid depth  $H$  is decreased and hence  $\delta_i$  increased while other parameters are fixed. Initially the fluid depth  $H$  is set to 6000m. For this parameter

the model exhibits a steady solution, symmetric about the middle latitude of the basin. When we decrease the depth  $H$  the circulation becomes stronger. For  $H$  around 5000m, the solution becomes asymmetric and has the subtropical gyre stronger than the subpolar gyre. The subtropical and subpolar recirculation vortices form an asymmetric dipole.

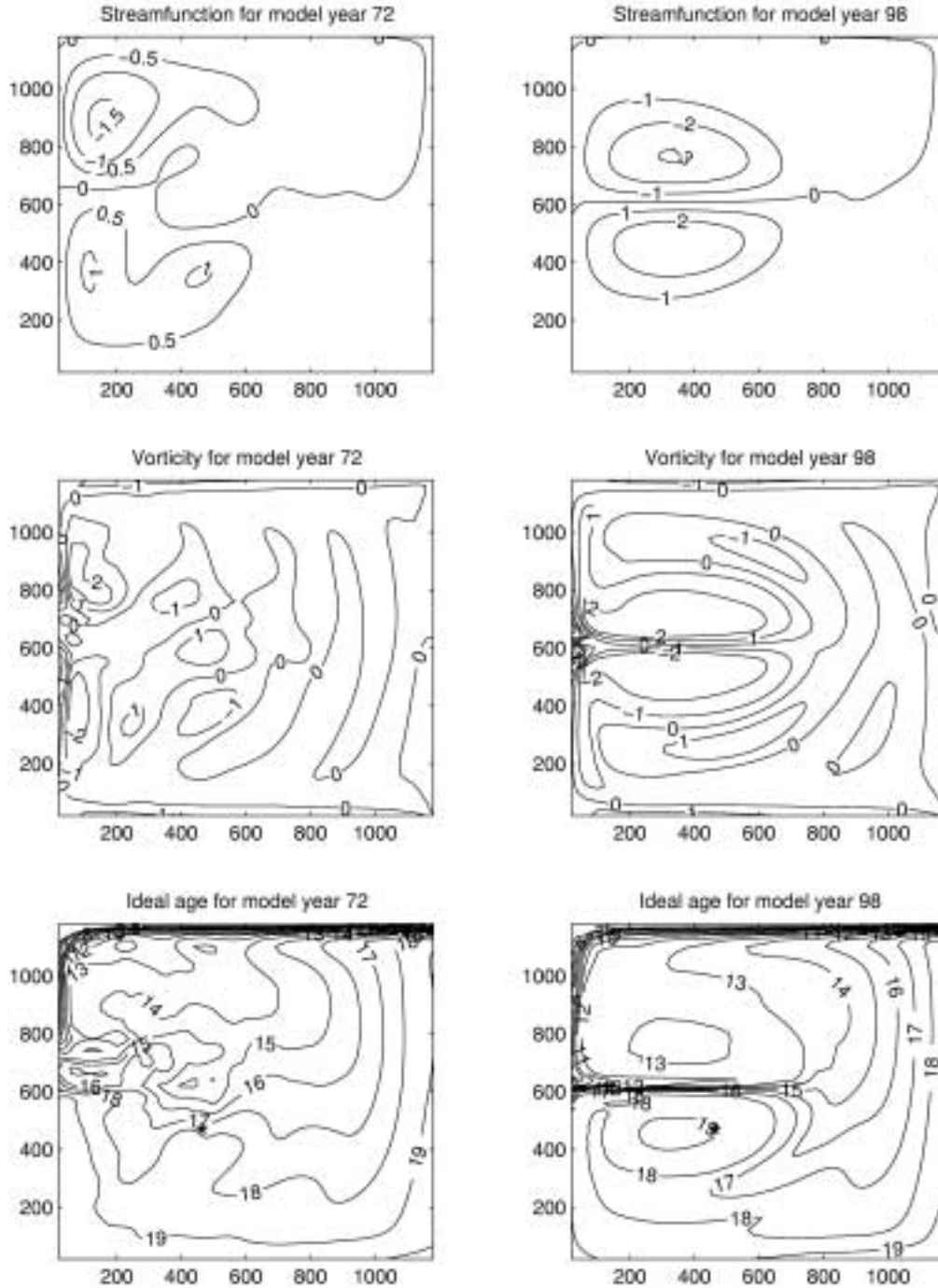


Fig 1 Streamfunction ( $10^6 \text{m}^2 \text{s}^{-1}$ ), vorticity ( $10^{-6} \text{s}^{-1}$ ) and ideal age (yr) of the unsteady circulation for model yr 72 and yr 98. The domain is 1200km on each side. The star shows the location of the timeseries in Fig. 2.

The circulation is still steady. As  $H$  is decreased to 4500m, the steady solutions lose their stability and become periodic. After  $H$  is decreased to 3500m, the periodic solution becomes aperiodic. At this value, the flow pattern is weakly chaotic. If  $H$  is further decreased, it becomes more and more chaotic.

Here, we focus on two flows: the steady flow with  $H=6000\text{m}$  and the chaotic flow with  $H=2500\text{m}$ . Fig. 1 shows two snapshots of the flow pattern of the unsteady circulation for model yr 72 and model yr 98 (streamfunction and vorticity). The flow for yr 72 has more eddies than the other while the latter is more symmetric about the mid-basin axis. Both the streamfunction and the vorticity fields exhibit similar features.

### 3. TRACER SIMULATIONS

A tracer model is combined with the dynamical model and tracers are transported by the instantaneous flow, i.e., advected by the large-scale flow field and diffused by the action of small-scale processes. The tracer advection-diffusion equation is

$$\left( \frac{\partial}{\partial t} + L \right) C = Q$$

where  $C$  is the tracer concentration,  $L$  the transport operator and  $Q$  source/sink term. Tracer is put into the basin at the northern boundary. Both transient tracers (linear-growth rate and exponential-growth rate) and steady tracers (with internal decay) are simulated in the gyre model. Simulations of ideal age tracer are also implemented. The source function  $Q$  in tracer transport equation corresponding to these tracers is defined in Table 2. The initial conditions (I.C.) and boundary conditions (B.C.) are also listed.

TABLE 2 Tracer and corresponding  $Q$ , I.C. and B.C.

Tracers	Source $Q$	I.C.	B.C.
Linear	$Q=0$	$C=0$	$C=t$
Exponential	$Q=0$	$C=0$	$C=\exp(t)$
Radioactive	$Q=-\lambda C$	$C=0$	$C=1$
Ideal age	$Q=1$	$C=0$	$C=0$

First we simulate idealized tracers in steady circulation and find the tracer ages and age spectrum are consistent with the tracer transport theory. Next we focus on unsteady circulation. Fig. 1 also shows the age map of the ideal age tracer for model yr 72 and model yr 98 (The age patterns of other tracers are very similar). The age pattern is consistent with its corresponding flow pattern. For yr 98, the flow pattern is somewhat symmetric and the age pattern has the same feature. We find two homogenization regions corresponding to the two gyres. For yr 72, there are some small eddies in the circulation and the age pattern is not so smooth.

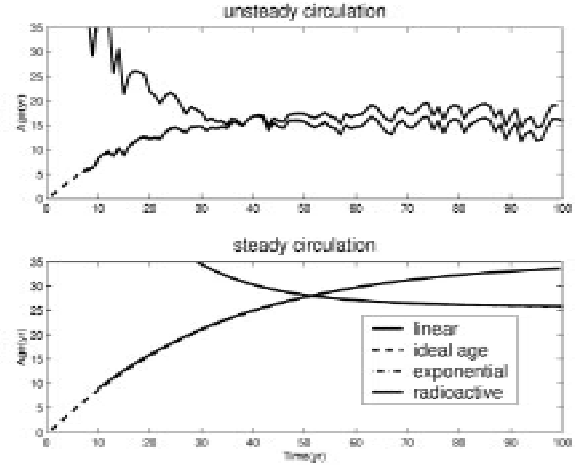


Fig 2 Time series of tracer ages at the location indicated in Fig. 1 for steady circulation and unsteady circulation.

Although the overall age patterns are very similar among different tracers, we can still find differences. Fig. 2 shows the time series of different tracer ages at one location indicated in Fig. 1. For all tracer ages, after experiencing a dramatic transient state they reach a statistically stationary state. Some tracer ages are nearly identical. The radioactive age is younger than the ideal age but they have the same tendency and peak-to-peak relationship as they are determined by the same circulation. For comparison, Fig. 2 also includes the time series of the tracer ages for steady circulation. The tracer ages in steady circulation are younger than those in unsteady circulation as the unsteady circulation is stronger. The ideal age is almost identical to the linear-growth tracer age and the radioactive age is almost identical to the exponential-growth tracer age for both steady circulation and unsteady circulation. For unsteady circulation, there is not only spatial variability (Fig. 1) but also temporal variability (Fig. 2) in tracer fields. In fact, the variability of the flow and the variability of the tracer fields are closely connected.

We examine this issue by analyzing the relationships between tracer and dynamical fields for the last 50 years. Fig. 3 shows the map of the correlation coefficient of the ideal age and vorticity. There are high (negative) correlation regions in the subtropical gyre but low correlation in the subpolar gyre. To examine these features further, we analyze the standard deviations of the flow and tracer fields. The main variability is concentrated in the western side of the inter-gyre regions (not shown). Accordingly, we choose four locations to examine the time evolution, where each location has different variability. The four locations (A,B,C,D) are indicated in Fig. 3 and the corresponding time series of the normalized ideal age and vorticity are in Fig. 4. There is high correlation at A and B but low correlation at C and D.

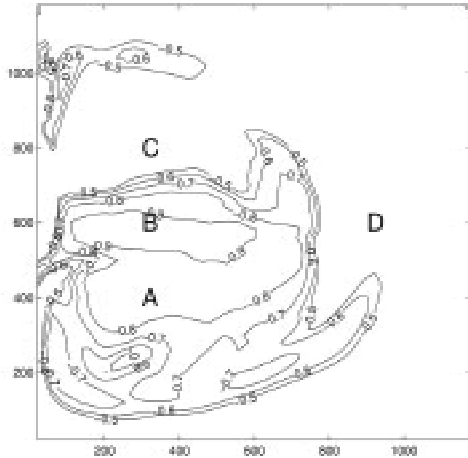


Fig 3 Pointwise correlation coefficient between ideal age and vorticity for the last 50 years. Only statistically significant correlations are shown.

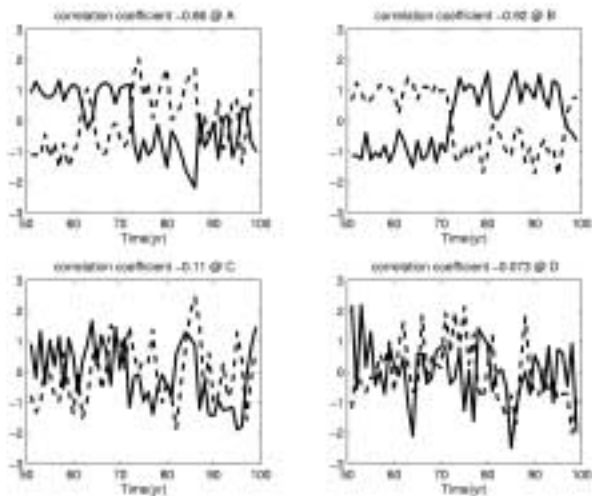


Fig 4 Time series of normalized vorticity (solid line) and ideal age (dashed line). C and D are not statistically correlated.

#### 4. CONCLUSION AND DISCUSSION

We have examined the transport in a simple barotropic double gyre circulation using several idealized tracers. Results show that for steady circulation, tracer ages are consistent with the tracer transport theory. Tracer age relationships that are well understood in steady circulation appear to hold in unsteady flow too. In unsteady flow, tracer ages show both spatial and temporal variability and there exist interesting relationships between tracer and dynamical fields.

Several issues arise from this study. One is why the age/vorticity correlation is low in the subpolar region. Also, how does the correlation apply to the real ocean and atmosphere, e.g., CFC12 tracer age and potential vorticity in the ocean. We are now working on these questions.

#### 5. REFERENCES

- Chang, K.I., et al., 2001: Transition to aperiodic variability in a wind-driven double-gyre circulation model, *J. Phys Oceanogr.*, **31**, 1260-1286.
- England, M.H., and E. Maier-Reimer, 2001: Using chemical tracers to assess ocean models, *Rev. Geophys.*, **39**, 29-70.
- Ghil, M., et al., 2002: Baroclinic and barotropic aspects of the wind-driven ocean circulation, *Physica D*, **167**, 1-35.
- Haine, T.W.N., and T.M. Hall, 2002: A generalized transport theory: Water-mass composition and age, *J. Phys Oceanogr.*, **32**, 1932-1946.
- Hall, T.M., and R.A. Plumb, 1994: Age as a diagnostic stratospheric transport, *J. Geophys. Res.*, **99**, 1059-1070.
- \_\_\_\_\_, and T.W.N. Haine, 2002: On ocean transport diagnostics: the idealized age tracer and the age spectrum, *J. Phys Oceanogr.*, **32**, 1987-1991.
- Holzer, M., and T.M. Hall, 2000: Transit-time and tracer-age distribution in geophysical flows, *J. Atmos. Sci.*, **57**, 3539-3558.
- Marshall, J., et al., 1997: A finite volume, incompressible Navier-Stokes model for studies of the ocean on parallel computers, *J. Geophys. Res.*, **102**, 5753-5766.
- Meacham, S.P., 2000: Low-frequency variability in the wind-driven circulation, *J. Phys Oceanogr.*, **30**, 269-293.
- Pedlosky, J., 1996: *Ocean Circulation Theory*, Springer-Verlag, 453pp.
- Siedler, G., et al., 2001: *Ocean Circulation and Climate: Observing and Modeling the Global Ocean*, Academic Press, 715pp.
- Waugh, D.W., and T.M. Hall (2002): Age of stratospheric air: Theory, observation and models, *Rev. Geophys. Res.*, **40**, 10.1029/2000RG000101.
- \_\_\_\_\_, et al., (2002): Relationships among tracer ages, to appear in *J. Geophys. Res.*